

Insights into Rare-Earth Metal Complex-Mediated Hydroamination

Shuqi Dong,[#] Jinjin Chen,[#] Kening Qiao, Jian Fang, Yan Yang, Laurent Maron,^{*} and Bo Liu^{*}Cite This: *ACS Catal.* 2021, 11, 3790–3800

Read Online

ACCESS |



Metrics & More



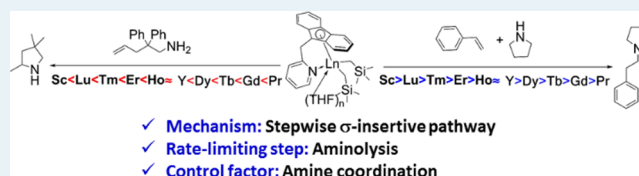
Article Recommendations



Supporting Information

ABSTRACT: Since the precise understanding of the underlying mechanism is important for the rational design of catalysts, much attention has been paid for hydroamination reactions catalyzed by organolanthanides during the past three decades. Distinct mechanisms were proposed on the basis of some key experimental features. It is a challenge to distinguish these mechanisms. The present study focuses on this controversial topic by synthesizing an almost entire range of rare-earth metal bisalkyl complexes (Py-CH₂-Flu)Ln(CH₂SiMe₃)₂(THF)_x (Ln = Sc (1), Lu (2), Tm (3), Er (4), Ho (5), Y (6), Dy (7), Tb (8), Gd (9), and Pr (10)) stabilized by a pyridine methylene fluorenyl ligand to catalyze intramolecular hydroamination (IAHA) of prototypical 1-amino-2,2-diphenyl-4-pentene and intermolecular hydroamination (IEHA) of styrene and pyrrolidine. Among them, thulium-, terbium-, and gadolinium-based catalysts were investigated for the first time. As observed for all the reported catalytic systems, the rate of IAHA increased almost linearly with increasing metal ion radius, whereas the reactivity pattern in IEHA with respect to the ionic radius size follows the opposite trend. Kinetic studies were carried out to obtain the empirical rate law $v = k[\text{Ln}]^{1.0}[\text{S}]^{0.0}$ for IAHA and $v = k[\text{Ln}]^{1.0}[\text{St}]^{1.0}[\text{pyrrolidine}]^{0.0}$ for IEHA. The zero-order dependence on amine was attributed to the population ratio between the rare-earth metal amido adduct and its precursor being larger than 10⁴. Density functional theory studies on scandium, yttrium, and praseodymium complex-mediated IAHA and IEHA were investigated using a stepwise σ -insertive mechanism and a concerted noninsertive mechanism, respectively. The results suggested the prevailing mechanism to be a stepwise σ -insertive pathway that involves the insertion of C=C into the Ln–N bond and protonolysis of the Ln–C bond. The protonolysis reaction is the turnover-limiting step. The reason behind the influence of the metal ion radius on the catalytic activity was elucidated.

KEYWORDS: hydroamination, rare-earth metal complexes, stepwise σ -insertive mechanism, DFT calculation, kinetic study



INTRODUCTION

The hydroamination reaction offers an atom-economical route to prepare nitrogen-containing fine chemicals and pharmaceuticals or construct useful chiral building blocks. However, this seemingly simple reaction is hampered by a high activation barrier derived from an electrostatic repulsion between the nitrogen lone pair of the amine and the olefinic π -bond. More importantly, the activation barrier cannot be overcome by increasing the reaction temperature because the negative reaction entropy results in the equilibrium preferring to shift the starting materials.¹ Significant research efforts have been paid to explore efficient catalysts. Catalytic systems based on transition metals^{2,3} and main group metals,^{4–7} as well as Brønsted acids,^{8,9} have been mainly developed. In 1989, Marks and his group were the first to discover the ability of lanthanocene precatalysts to efficiently promote the intramolecular hydroamination (IAHA) of aminoalkene derivatives. Then, they employed the same catalytic systems to successfully catalyze the intermolecular hydroamination (IEHA) of alkenes and alkynes, which is significantly more challenging since acetylenic and olefinic substrates compete weakly with amines for vacant coordination sites at the active metal center.¹⁰ These landmark studies stimulated a new direction for exploring catalysts.¹¹ Ten years later, Livinghouse and Bercaw extended

the catalysts to simple noncyclopentadienyl lanthanide trisamides, promoting the considerable development of rare-earth metal-based catalysts.¹²

IAHA of aminoalkenes catalyzed by rare-earth metal complexes has attracted most of attention. It has been demonstrated that organolanthanides are highly efficient and selective catalysts for the IAHA of various C–C unsaturations such as aminoalkenes,^{13–37} aminoalkynes,^{38–43} aminoalkenes,^{44–46} and aminodienes.^{47–49} A probable stepwise σ -insertive mechanism (Scheme 1 A) that comprises a turnover-limiting insertion of a C–C multiple bond into the Ln–N bond linked to rapid aminolysis of the resulting Ln–C bond was proposed on the basis of the following observations: (1) the increased ionic radius and improved coordination sphere result in increasing turnover frequencies (TOFs) common in lanthanide-catalyzed olefin transformations, suggesting that TOF is sensitive to olefin insertion; (2) the kinetic study

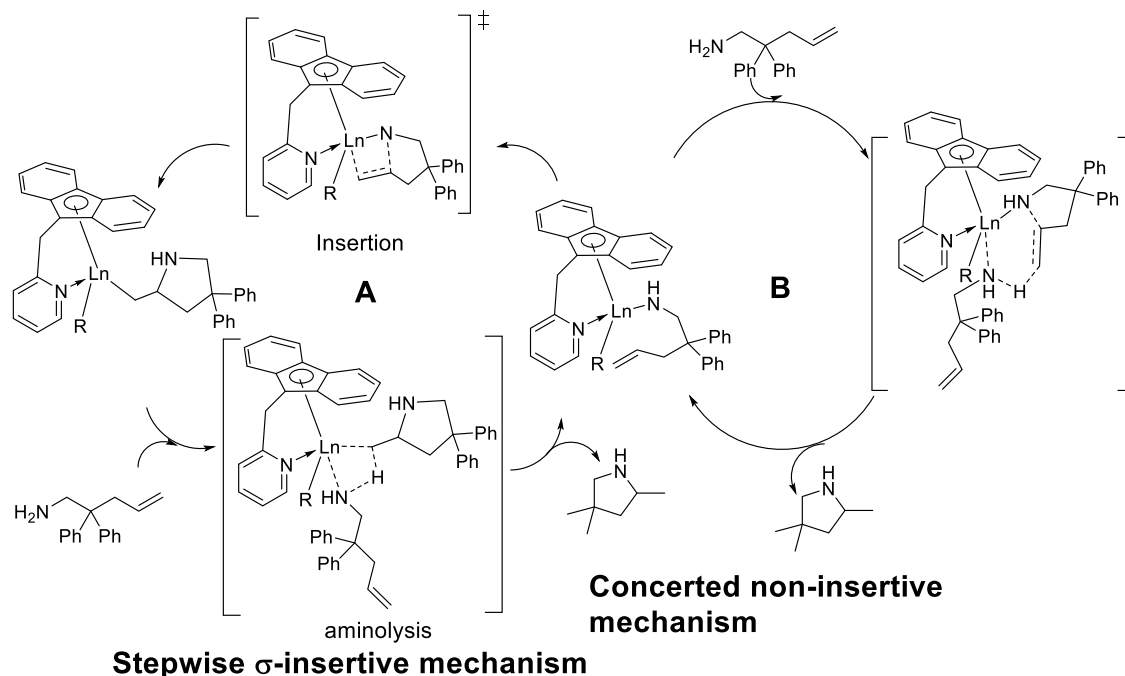
Received: February 5, 2021

Revised: March 2, 2021

Published: March 12, 2021



Scheme 1. Proposed Mechanisms for IAHA catalyzed by a Rare-Earth Metal Complex



revealed the rate to be first order in organolanthanides and zero order in aminoalkenes, arguing that the influence of aminolysis on the whole process is trivial. While in some cases, a distinctive aminoalkene-dependent first-order kinetic profile was observed even up to high conversions. In particular, rare-earth bis(amidoalkene) compound $[\{Cp^*PN\}Y-(NHCH_2CMe_2CH_2CH=CH_2)_2]$ was isolated through a reaction of $\{Cp^*PN\}Lu(CH_2SiMe_3)_2$ with 1.6 equiv of 2,2-dimethylpenten-4-ylamine and no cyclization was observed without additional amine substrates. These discoveries led to another concerted noninsertive mechanism (Scheme 1 B) with a six-centered transition state involving concerted C–N and C–H bond formation.^{30,50} Does the mechanism vary case by case or one of them represent the truth?

In contrast to the IAHA, IEHA has aroused less attention. A few catalytic systems were reported to be active toward IEHA.^{25,43,51–54} Among them, only lanthanocene⁵¹ and binaphtholate rare-earth metal complexes^{52,53} as precatalysts were investigated systematically. When employing lanthanocenes to catalyze IEHA, the TOF diminishes with a constricting metal ion coordination sphere, in accord with documented steric requirements for the insertion of olefinic functionalities into lanthanide-alkyl and lanthanide-heteroatom σ -bonds, suggesting that intermolecular C–C multibond insertion into the Ln–N bond is the turnover-limiting step. However, a converse trend was observed on adopting binaphtholate rare-earth metal complexes as precatalysts. The reason behind this is unclear.

Computational studies could reveal information that is not available from experimental methods. Initially, Marks and Fragala studied organolanthanide-mediated $(Cp_2LaCH(SiMe_3)_2)$ hydroamination processes of a prototypical aminoalkene, $NH_2(CH_2)_3CH=CH_2$, by analyzing the stabilities and geometries of reactants, intermediates, and products within the cyclization and protonolysis steps.⁵⁵ Since all energy values related to protonolysis lie lower than those of the reactants, especially, the corresponding energy of the transition state lies

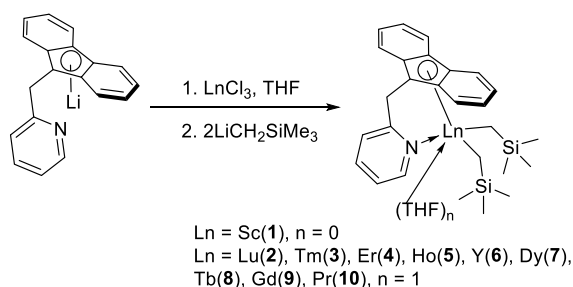
12.6 kcal/mol lower than the energy of the insertion transition state, a conclusion was made that the insertion of an olefin into the Ln–N bond is the rate-limiting step even the energetic barrier of protonolysis is 0.9 kcal/mol higher than that of olefin insertion. Then, Tobisch scrutinized organolanthanide-mediated $Cp^*_2LaCH(SiMe_3)_2$ IAHA of (4*E*,6)-heptadien-1-amine by calculating the condensed free-energy profile for individual elementary steps of the overall reaction.⁵⁶ On the basis of the fact that the protonolysis step has the highest energetic barrier, a mechanistic scenario was proposed that the olefin insertion is facile, while protonation is the rate-limiting step. Both of them suggested the rate-limiting step but unfortunately these results are not consistent.

Herein, we found that with the increasing metal size, the catalytic activity of pyridine methylene fluorenyl-ligated rare-earth metal bisalkyl species toward IAHA of 1-amino-2,2-diphenyl-4-pentene increased, while a converse trend was observed for IEHA of styrene and pyrrolidine. A density functional theory (DFT) calculation was employed to unveil the reasons behind; meanwhile, the above unsolved mysteries were attempted to be addressed.

RESULTS AND DISCUSSION

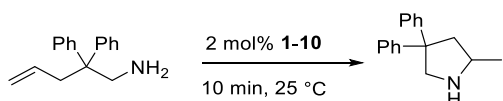
Very recently, we synthesized the entire range of rare-earth metal bisalkyl complexes $(Py-CH_2-Flu)Ln-(CH_2SiMe_3)_2(THF)_x$ (Scheme 2) ($Ln = Sc$ (1), Lu (2), Tm (3), Er (4), Ho (5), Y (6), Dy (7), Tb (8), Gd (9), and Pr (10)) except lanthanum stabilized by a pyridine methylene fluorenyl ligand via a metathesis reaction between the lithium salt $(Flu-CH_2-Py)Li$ and $LnCl_3$ followed by a lithiation reaction with 2 equiv of Me_3SiCH_2Li .⁵⁷ Upon activation by $[Ph_3C][B(C_6F_5)_4]$ and Al^iBu_3 , complexes 1–9 showed high activity and syndioselectivity for styrene polymerization, while the large Pr-attached precursor 10 exhibited slightly dropped syndioselectivity but a rather low activity. The activity increased with the decrease of the rare-earth metal size, in striking contrast to the literature studies that a large-sized

Scheme 2. Synthesis of Rare-Earth Metal Alkyl Complexes 1–10



metal exhibits high activity toward olefin transformations. This prompted us to investigate their behavior on the hydroamination reaction. The IAHA reaction of 1-amino-2,2-diphenyl-4-pentene was scrutinized. In the presence of 2 mol % of complex **1**, 7% conversion was achieved within 10 min at 25 °C (Table 1, entry 1). This is the rare scandium complex

Table 1. IAHA Reactions Catalyzed by Complexes 1–10^a



entry	complex	yield/% ^b	TOF/h ^{-1c}
1	1	7	21
2	2	23	69
3	3	35	105
4	4	46	138
5	5	57	171
6	6	57	171
7	7	68	204
8	8	75	225
9	9	81	243
10	10	100	297

^aLn: 10 μmol, C₆D₆: 0.6 mL, [aminoalkene]₀: [Ln]₀ = 50:1, temperature: 25 °C, time: 10 min. ^bDetermined from ¹H NMR spectrum. ^cTOF = 50*yield/10*60.

that successfully catalyzed IAHA at an ambient temperature, although the activity was not very high.^{23,25,35,50,58–61} Under the same conditions, lutetium complex **2** showed a much higher activity. The TOF reached 69 h⁻¹ (Table 1, entry 2). Complex **3** is the first example of a thulium-based catalyst to be used for the IAHA reaction. The TOF was over 10² h⁻¹ (Table 1, entry 3). **4** exhibited an activity one order of magnitude higher than the only reported erbium complex with a tridentate silicon-linked amido-indenyl ligand (15 h⁻¹)⁶² (Table 1, entry 4). The holmium complex **5** and the yttrium complex **6** showed similar activities (Table 1, entries 5 and 6). This phenomenon was similar to that observed in the IAHA reaction catalyzed by bis(phosphinimino)methanide rare-earth metal complexes.⁶³ Compared to the reported dysprosium complexes,^{16,27} complex **7** could catalyze IAHA to achieve high conversion under relatively mild conditions (Table 1, entry 7). Surprisingly, although more than one hundred papers related to IAHA catalyzed by rare-earth metal species were published, the terbium and gadolinium complexes had never been tested in the IAHA reaction. Thus, complexes **8** and **9** were, respectively, the first discovery (Table 1, entries 8 and 9). The praseodymium complex **10** could quantitatively convert 50

equiv of 1-amino-2,2-diphenyl-4-pentene into 2-methyl-4,4-diphenylpyrrolidine within 10 min (Table 1, entry 10). Complex **10** showed the highest catalytic activity even when the reaction time was not optimized. As observed for all the reported catalytic systems,^{14,24,38,60,63–66} the rate increased almost linearly with the increasing metal ion radius (Figure 1). The deviation of scandium complex **1** might be attributed to the negative effect of metal size being compensated by the higher Lewis acidity of the metal center.

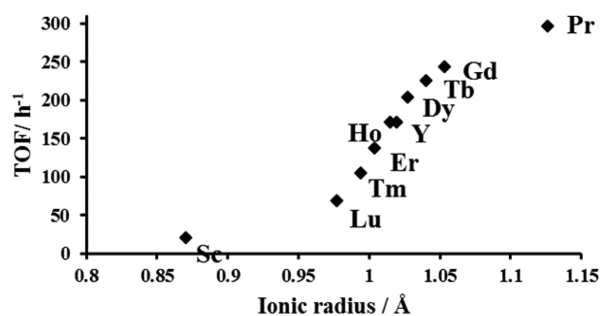
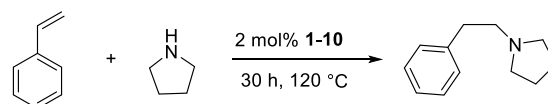


Figure 1. Plots of TOF for the hydroamination of 1-amino-2,2-diphenyl-4-pentene with complexes 1–10 as catalysts vs ionic radius of the center metals.

The IEHA of styrene and pyrrolidine was also investigated. Interestingly, the scandium complex **1** showed the highest catalytic activity; meanwhile, compared to that for IAHA, the TOF for IEHA still decreased twenty times (Table 2, entry 1).

Table 2. IEHA Reactions Catalyzed by Complexes 1–10^a



entry	complex	yield/% ^b	TOF/h ^{-1c}
1	1	63	1.05
2	2	53	0.88
3	3	50	0.83
4	4	48	0.80
5	5	46	0.76
6	6	45	0.75
7	7	30	0.50
8	8	27	0.45
9	9	20	0.33
10	10	7	0.11

^aLn: 10 μmol, [styrene]₀: [pyrrolidine]₀: [Ln]₀ = 50:50:1, temperature: 120 °C, time: 30 h. ^bDetermined from ¹H NMR spectrum. ^cTOF = 50*yield/30.

It is worth noting that IEHA proceeds in the presence of an equivalent amount of styrene and pyrrolidine. This is different from IEHA catalyzed by metallocene lanthanide complexes where large excess of styrene is necessary to minimize the amine inhibition.⁵¹ With the metal size increasing, the catalytic activity decreased gradually from 0.88 to 0.33 h⁻¹ (Table 2, entries 2–9). The TOF of praseodymium complex **10** is a tenth of that of the scandium complex **1** (Table 1, entry 10). This is in striking contrast to that observed for the metallocene lanthanide catalysts, where the neodymium complex showed the highest TOF, which is one hundred times the lowest one obtained for the lutetium complex.⁵¹ The reactivity pattern in

IAHA and IEHA reactions with respect to the ionic radius size follows the opposite trend to that observed for hydroamination reactions catalyzed by alkaline earth metal species.^{67–69}

Kinetic study. Kinetic studies of IAHA of 1-amino-2,2-diphenyl-4-pentene catalyzed by the pyridine methylene fluorenyl-ligated lutetium complex were carried out at 25 °C. The plot of substrate conversion versus reaction time gives a straight line, while a deviation is observed at a higher substrate conversion (>50%) (Figure 2). In contrast, the semi-

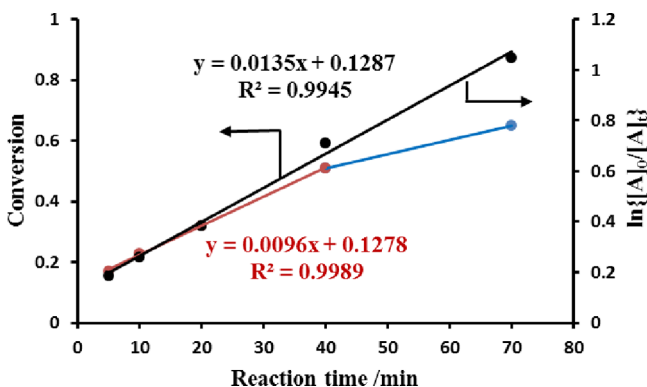


Figure 2. Plot of substrate conversion and $\ln\{[A]_0/[A]_t\}$ vs reaction time for IAHA of 1-amino-2,2-diphenyl-4-pentene (A) using complex 2 as a precursor ($[2]_0 = 4$ mM, $[S]_0 = 80$ mM, 25 °C, C_6H_6).

logarithmic plot of substrate conversion versus reaction time yields a straight line with a good R^2 value over the full range of conversion, suggesting a first-order dependence on substrate (Figure 2). On the surface, the order of the substrate plays an important role in determining the mechanism since a stepwise σ -insertive mechanism of IAHA was proposed on the basis of the reaction being zero order in aminoalkenes, while a proton-assisted concerted N–C/C–H bond-forming mechanism was derived from the fact that the reaction is first order in the substrate. Thus, the rate dependence on the substrate concentration was examined by varying the initial concentration of 1-amino-2,2-diphenyl-4-pentene (A) in the range of 80–300 mM using complex 2 as a precursor (Figure 3). The values of k_{obs} extracted from the semilogarithmic plot of conversion versus reaction time decreased slightly with the increasing initial substrate concentration, from $k_{obs} = 1.35 \times 10^{-2} \text{ min}^{-1}$ for $[S]_0 = 80$ mM slightly down to $1.31 \times 10^{-2} \text{ min}^{-1}$ for $[S]_0 = 150$ mM. This confirmed the zero-order

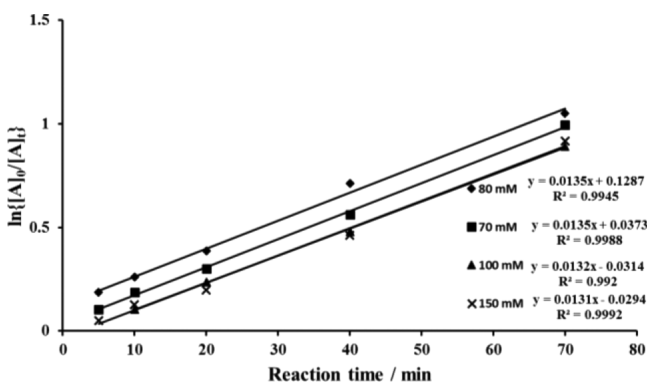


Figure 3. Plot of $\ln\{[A]_0/[A]_t\}$ vs reaction time for IAHA of 1-amino-2,2-diphenyl-4-pentene (A) catalyzed by complex 2 at 25 °C at different concentrations of the substrate (C_6H_6 , 25 °C, $[2]_0 = 4$ mM).

dependence on the substrate. The deviation from zero-order kinetics at higher substrate conversion might be attributed to the coordination of the Lewis basic product, leading to competitive product inhibition (Figure 2). This result is consistent with the catalytic behavior of ansa-lanthanocenes and constrained geometry lanthanide systems.³⁸ The rate dependence on catalyst concentration was also examined by varying the initial concentration of 2 in the range of 2.5–20.0 mM while keeping $[S]_0$ constant (0.25 M) (Figure 4). The

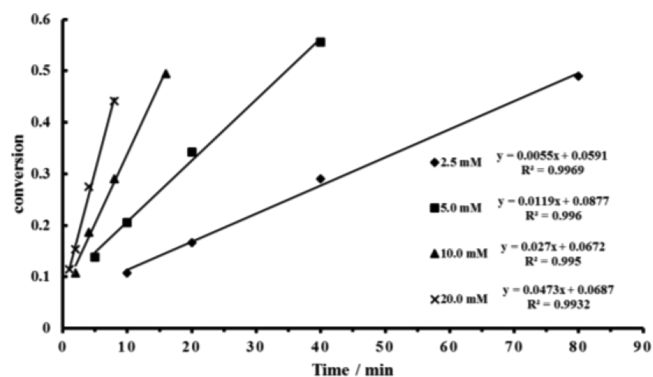


Figure 4. Plot of substrate conversion vs reaction time for IAHA of 1-amino-2,2-diphenyl-4-pentene (A) catalyzed by complex 2 at 25 °C at different concentrations of complex 2.

plot of $\ln(k_{obs})$ versus $\ln([2]_0)$ was a line with a slope of 1.05 ($R^2 = 0.9941$) (Figure 5). This was characteristic of a first-

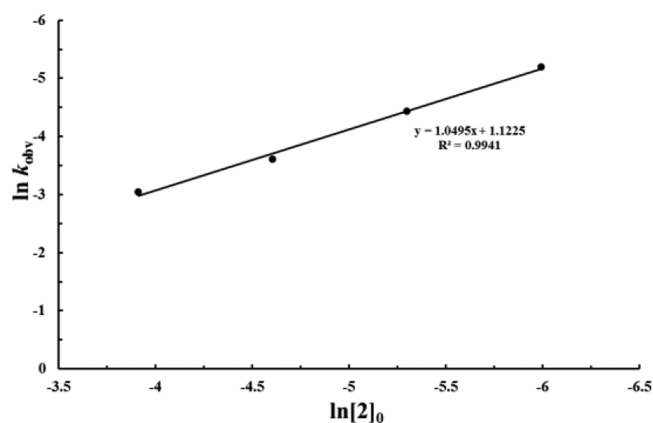


Figure 5. Plot of $\ln(k_{obs})$ vs $\ln[2]_0$ for the IAHA of 1-amino-2,2-diphenyl-4-pentene (A) catalyzed by complex 2.

order dependence on catalyst concentration. Therefore, the IAHA catalyzed by the pyridine methylene fluorenyl-ligated rare-earth metal complex obeyed the empirically determined rate law given in eq 1

$$v = k[\text{Ln}]^{1.0}[\text{S}]^{0.0} \quad (1)$$

Meanwhile, the kinetic behavior of IEHA of styrene and pyrrolidine catalyzed by complex 2 was also investigated. The molar ratio of styrene to pyrrolidine was held at 1:1. Thus, the rate law was simplified to eq 2.

$$v = k[\text{Ln}]^a[\text{S}]^b \quad (2)$$

The plots of styrene conversion (C) and $C/(1-C)$ versus reaction time are nonlinear, excluding a zero-order or second-order dependence on the substrate, that is, $b \neq 0$ and 2 (Figure

6). A first-order kinetic plot ($\ln\{[S]_0/[S]_t\}$ vs reaction time) is shown in Figure 7, indicating $b = 1$, that is, a first-order

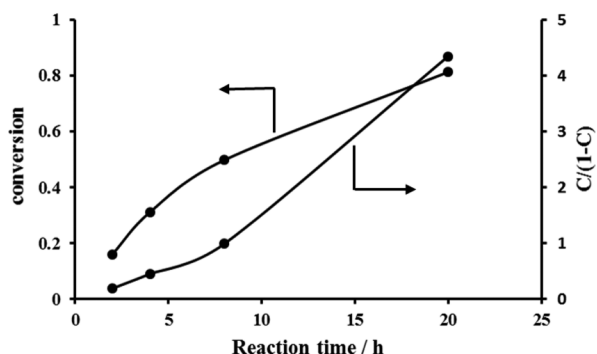


Figure 6. Plot of styrene conversion (C) and $C/(1-C)$ vs reaction time for IEHA of styrene and pyrrolidine catalyzed by complex 2 with the ratio of styrene to pyrrolidine being 1:1 (C_6D_6 , $120\text{ }^\circ\text{C}$, $[2]_0 = 0.27\text{ M}$, $[styrene]_0 = [pyrrolidine]_0 = 4.5\text{ M}$).

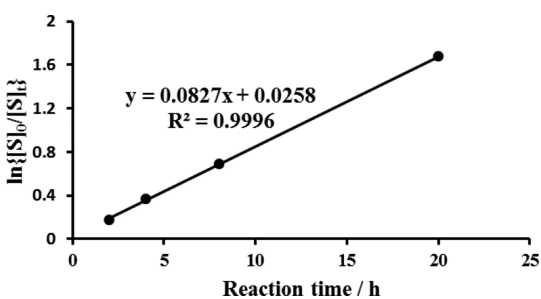


Figure 7. Plot of $\ln\{[S]_0/[S]_t\}$ vs reaction time for IEHA of styrene and pyrrolidine catalyzed by complex 2 with the ratio of styrene to pyrrolidine being 1:1 (C_6D_6 , $120\text{ }^\circ\text{C}$, $[2]_0 = 0.27\text{ M}$, $[styrene]_0 = [pyrrolidine]_0 = 4.5\text{ M}$).

dependence on styrene concentration and a distinctive zero-order dependence on pyrrolidine concentration. The rate dependence on the catalyst concentration was examined by varying the initial concentration of 2 in the range of 0.04–0.27 M while keeping $[S]_0$ constant (4.5 M) (Figure 8). The plot of $\ln(k_{obs})$ versus $\ln([2]_0)$ was a line with a slope of 1.02 ($R^2 = 0.9952$) (Figure 9). This was characteristic of a first-order

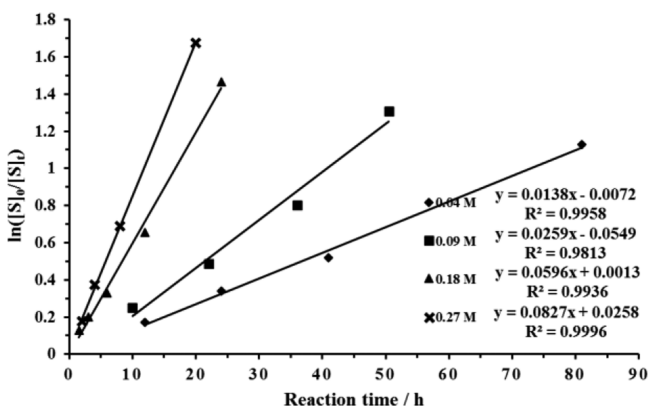


Figure 8. Plot of substrate conversion vs reaction time for IEHA of styrene and pyrrolidine catalyzed by complex 2 at $120\text{ }^\circ\text{C}$ at different concentrations of complex 2 (C_6D_6 , $120\text{ }^\circ\text{C}$, $[styrene]_0 = [pyrrolidine]_0 = 4.5\text{ M}$).

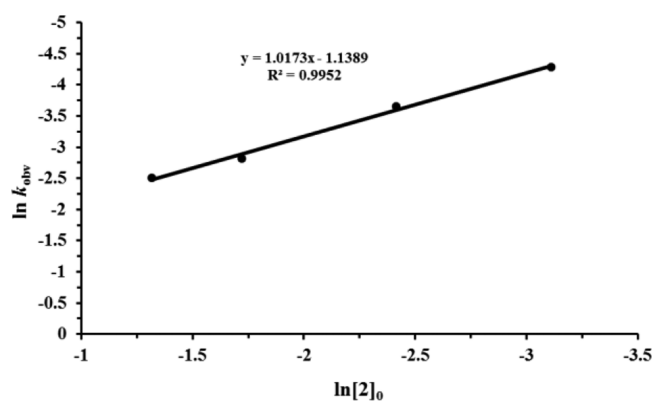


Figure 9. Plot of $\ln(k_{obs})$ vs $\ln[2]_0$ for the IEHA of styrene and pyrrolidine catalyzed by complex 2.

dependence on catalyst concentration. Therefore, the IEHA catalyzed by $(Py-CH_2-Flu)Ln(CH_2SiMe_3)_2(THF)_x$ obeyed the empirically determined rate law given in eq 3, which is the same as that established for ansa-lanthanocenes by Marks.⁵¹

$$v = k[Ln]^{1.0}[St]^{1.0}[pyrrolidine]^{0.0} \quad (3)$$

DFT Study of the reaction mechanism. A DFT study was conducted with the representative complexes 1, 6, and 10 using the hybrid functional B3PW91 (further details are included in the Supporting Information) since scandium possesses the smallest ionic radius, yttrium is located in the middle of the range of rare-earth metals, and praseodymium has the largest size.

First, the transformation of the metal bisalkyl complex into a catalytically competent rare-earth amido compound, that is, catalyst generation, was considered (Figure 10). The metal alkyl binds to a molecule of amine, forming a thermodynamically stable substrate adduct. After the substrate adduct $I\cdot A$ (or $I\cdot A'$) formation, the system evolves through a metathesis-type transition state TS_0 (TS'_0). Thereafter, the transition state of aminolysis decays into a substrate-free metal amido catalyst complex (II or II'). Complexation of an additional molecule of amine to II or II' is kinetically facile and downhill, leading to the most stable adduct species ($II\cdot A$ or $II\cdot A'$). The free-energy data of the intermediates and transition-state species of catalyst generation are summarized in Table 3. The aminoalkene adducts ($I\cdot A$) involved in the IEHA reaction are less stable than the pyrrolidine analogue ($I\cdot A'$) generated in the IEHA reaction due to the weak Lewis basicity of aminoalkenes. With the increasing metal size, the energy of the aminolysis transition state (TS_0 or TS'_0) decreases. In addition, the praseodymium amido complex adduct ($II\cdot A$ or $II\cdot A'$) is the most stable. The above results indicate that with the increase of the metal ion radius, catalyst generation becomes more favorable in both kinetic and thermodynamic aspects, which might be owing to the decrease of the Lewis acidity of the metal center. Moreover, the aminolysis of the metal alkyl complex by pyrrolidine is more facile than that by aminoalkene. The transformation of the second alkyl in the IEHA case was also computed and was found to be favorable (Figure S1), but since the barriers of the next steps of the full catalytic cycles were not affected (Figure S2), the discussion is based on the reactions starting from $II\cdot A$ and $II\cdot A'$.

Subsequently, the full catalytic cycle was computed using the stepwise σ -insertive mechanism and concerted noninsertive mechanism, respectively.

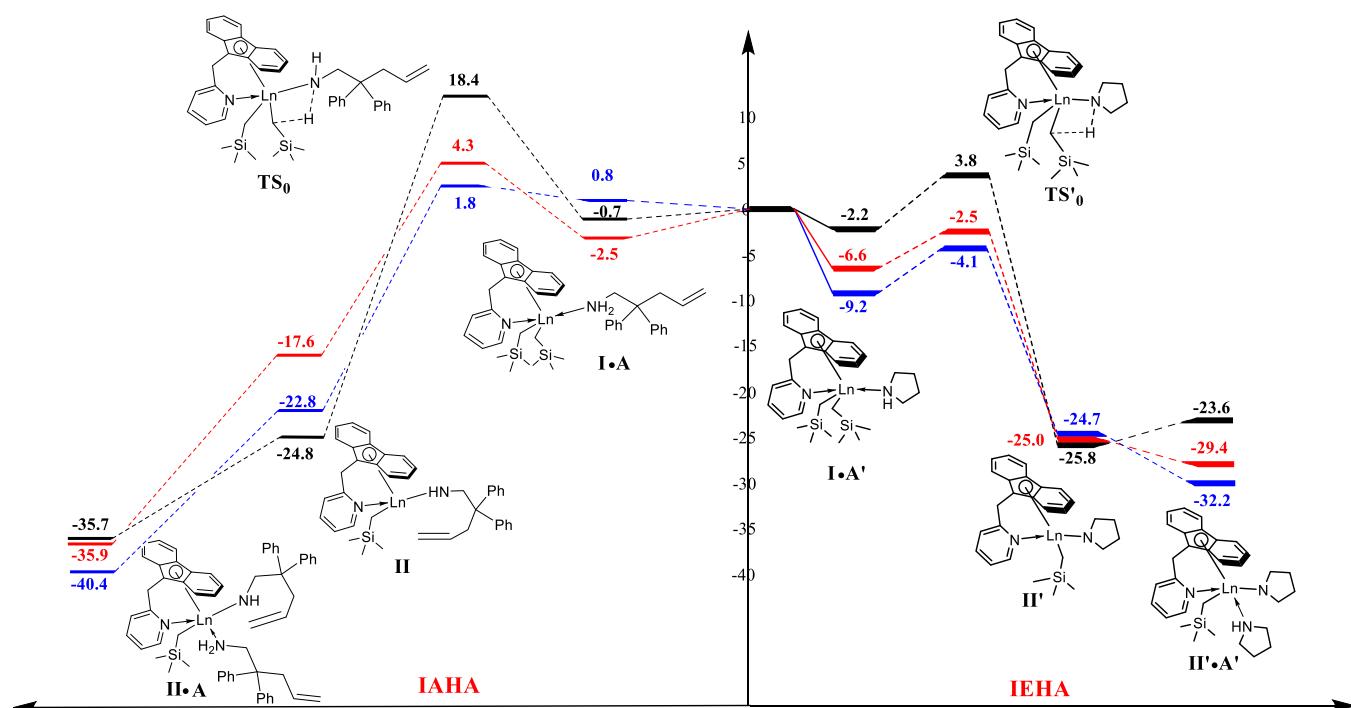


Figure 10. Catalyst generation profile at room temperature for IAHA (left) and IEHA (right) catalyzed by complex 1 (black), complex 6 (red), and complex 10 (blue) (kcal/mol at RT).

Table 3. Energy Data of the Intermediates and Transition-State Species of the Catalyst Generation Step

metal	amine adduct of I (kcal/mol)		transition state (kcal/mol)		amine adduct of II (kcal/mol)	
	I•A	I•A'	TS ₀	TS' ₀	II•A	II'•A'
Sc	-0.7	-2.2	18.4	3.8	-35.7	-23.6
Y	-2.5	-6.6	4.3	-2.5	-35.9	-29.4
Pr	0.8	-9.2	1.8	-4.1	-40.4	-32.2

For IAHA (Figure 11), the proton-assisted concerted N–C/C–H bond-forming pathway is seen to be energetically prohibitive compared to a kinetically less demanding σ -insertive pathway. Thus, only the σ -insertive pathway is discussed in detail. The latter can be split in two steps, namely, cyclization and protonolysis. Cyclization should be triggered by sufficiently effective activation of the olefin unit; however, the accessibility of the double bond to the metal center is blocked by the additional coordinated amine due to the crowded coordination environment around the metal

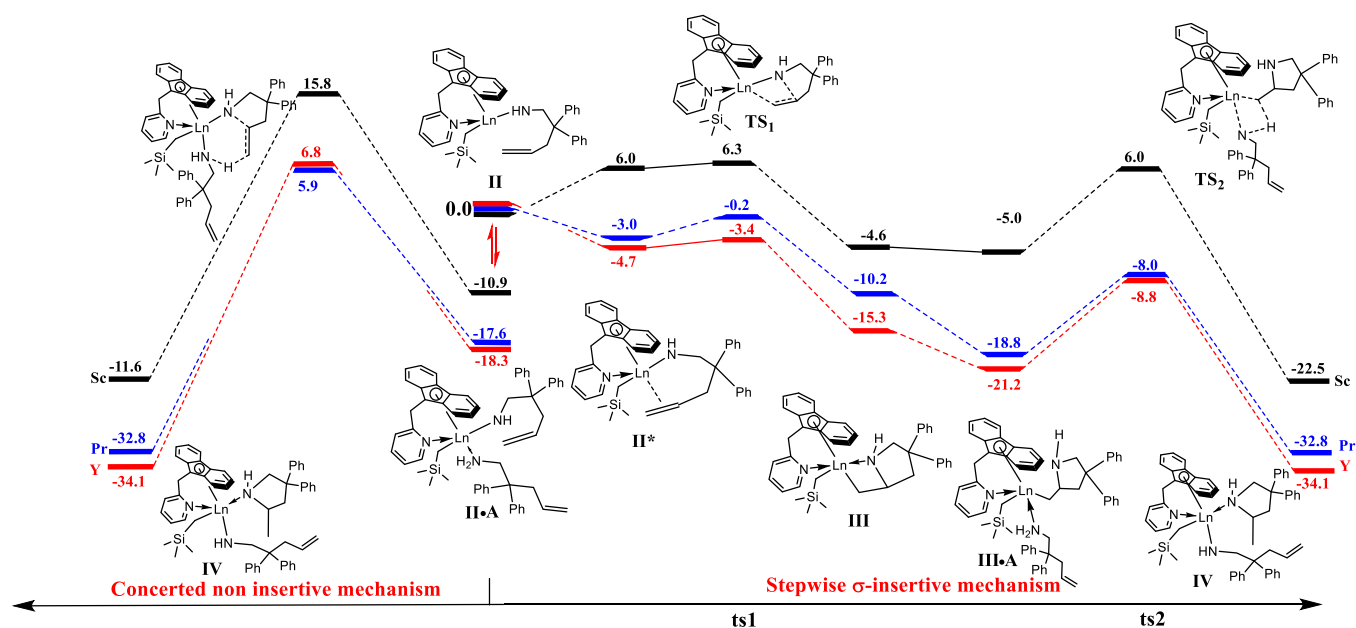


Figure 11. Catalytic cycle profile of IAHA of 1-amino-2,2-diphenyl-4-pentene catalyzed by complex 1 (black), complex 6 (red), and complex 10 (blue) using the concerted noninsertive mechanism (left) and stepwise σ -insertive mechanism (right) (kcal/mol at RT).

Table 4. Population Ratio between III·A (III'·A') and Its Precursor III (III')

metal	IAHA			IEHA		
	$\Delta G_{\text{III}\cdot\text{A}}$ (kcal/mol)	ΔG_{III} (kcal/mol)	$n_{\text{III}\cdot\text{A}}/n_{\text{III}}$ ^a	$\Delta G_{\text{III}'\cdot\text{A}'}$ (kcal/mol)	$\Delta G_{\text{III}'}$ (kcal/mol)	$n_{\text{III}'\cdot\text{A}'}/n_{\text{III}'}$
Sc	-5.0	-4.6	1.97	8.2	9.4	7.57
Y	-21.2	-15.3	2.15×10^4	-1.8	3.6	9.16×10^3
Pr	-18.8	-10.2	2.05×10^6	-8.4	0.8	5.63×10^6

^a $n_{\text{III}\cdot\text{A}}/n_{\text{III}}$ can be calculated in accordance with Boltzmann statistics

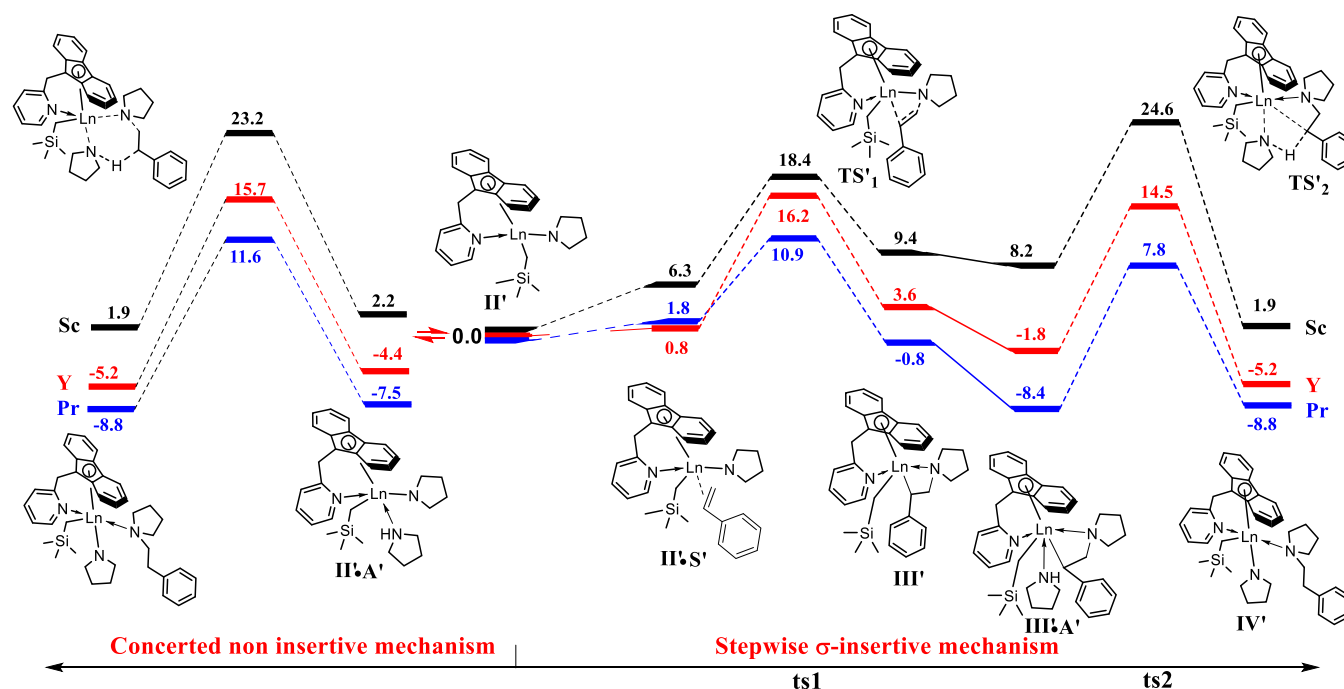


Figure 12. Catalytic cycle profile of IEHA of styrene and pyrrolidine catalyzed by complex 1 (black), complex 6 (red), and complex 10 (blue) using the concerted noninsertive mechanism (left) and stepwise σ -insertive mechanism (right) (kcal/mol at RT).

center since all attempts to locate the isomer of II·A with a double bond chelate were unsuccessful. Thus, the cyclization starts from the metal amido complex II. The isomerization of II into the activated species II* with a suitably attached double bond is thermodynamically favorable due to the chelating effect associated with the ligand-to-metal donation from the electron-rich C=C bond. However, the scandium species do not behave in the same way because of the steric effects (too crowded coordination sphere owing to its smallest ionic radius) (Table 4). Migratory olefin insertion into the metal–N σ -bond through TS₁ is facile with a minute barrier to overcome (Sc: 0.3 kcal/mol, Y: 1.3 kcal/mol, and Pr: 2.8 kcal/mol). The energy of the cyclization product (III) is lower than that of the activated species II*, and therefore, the process is considered exothermic, in accordance with the result observed in the IAHA of aminodienes catalyzed by a constrained geometry samarium complex.⁷⁰ An extra aminoalkene coordination to III is thermodynamically preferred, facilitating cyclization to form the most stable intermediate III·A. After cyclization, protonolysis occurs through a metathesis-type TS₂ structure that describes the cleavage of an already suitably polarized N–H bond and concomitant C–H bond formation. The activation barrier for protonolysis is determined to be 11.0 kcal/mol for the scandium-based catalyst, 12.4 kcal/mol for the yttrium-based catalyst, and 10.8 kcal/mol for the praseodymium-based precursor. All of them are comparable to the activation barriers for the lanthanocene precatalyst (12.8

kcal/mol)⁵⁵ and cyclopentadienyl-bis(oxazolonyl)-borate yttrium alkyl compound (10.0 kcal/mol)⁷¹ and higher than the corresponding activation barrier of cyclization, suggesting that protonolysis is the turnover-limiting step, although the energy of the protonolysis transition state TS₂ is lower than that of cyclization transition state TS₁. The activation barrier order of protonolysis follows a Y > Sc \approx Pr trend. This trend seems at first sight different from the experimental results Pr > Y > Sc. It is worth noting that the population ratio between III·A and its precursor III for the catalytic system based on yttrium and praseodymium is larger than 10⁴ (Table 4), suggesting that the substrate adduct can be easily formed even at extremely low substrate concentrations, while for the scandium-based catalytic system, the value of $n_{\text{III}\cdot\text{A}}/n_{\text{III}}$ is only 1.97, that is, 4–6 orders of magnitude lower than those calculated for the catalytic systems involving yttrium and praseodymium. Therefore, the concentration of III·A is rather low for the scandium species and therefore reduces the possibility of protonolysis reaction, resulting in the lowest activity of the scandium species. This result is consistent with the observation in IAHA catalyzed by a scandium complex that a deviation from zero-order kinetics at a higher substrate conversion is observed (Figure S3) and also could elucidate why a distinctive substrate-dependent first-order kinetic profile was observed in some cases. For example, Tobisch scrutinized the IAHA of NH₂CH₂C(Me)₂CH₂CH=CH₂ using a highly active cyclopentadienyl-bis(oxazolonyl)-borate {Cpo}Y^{III} alkyl compound

and found that the energy of the aminoalkene adduct species is 4.3 kcal/mol higher than that of its precursor,⁷¹ in accord with a first-order dependence on the concentration of aminoalkene observed by Sadow.³⁰

$$n_{\text{III}\cdot\text{A}}/n_{\text{III}} = \exp\left(-\frac{\Delta G(\text{III}\cdot\text{A})}{RT}\right) / \exp\left(-\frac{\Delta G(\text{III})}{RT}\right)$$

where $n_{\text{III}\cdot\text{A}}$ and n_{III} represent the populations of $\text{III}\cdot\text{A}$ and III , respectively, $\Delta G_{\text{III}\cdot\text{A}}$ and ΔG_{III} denote the Gibbs free energies of $\text{III}\cdot\text{A}$ and III , respectively, R is the gas constant, and T is the absolute temperature. $T = 298.15$ K is used here as the free energy is calculated at this temperature, which is also consistent with the experimental temperature (298 K).

For the IEHA (Figure 12), the noninsertive mechanism involves N–C ring closure triggered by concomitant amino proton delivery onto the adjacent C=C linkage, thereby affording a cyclamine product through a concerted single-step transformation. This process is seen to be energetically comparable to the σ -insertive pathway, but the order of the barrier for the N–C ring closure (Sc: 21.0 kcal/mol > Y: 20.1 kcal/mol > Pr: 19.1 kcal/mol) is opposite to the experimental result that the catalytic activity decreased with the increasing metal size. This precluded the proton-assisted concerted N–C/C–H bond-forming pathway. Thus, a detailed analysis was carried out for the classic σ -insertive pathway (Figure 12, right). The insertion starts from the coordination of styrene to the metal center of II' , which is endothermic. The population ratio of styrene adduct $\text{II}'\cdot\text{S}'$ to its precursor species II' is much lower than 1, suggesting that the formation of the styrene adduct is sensitive to the styrene concentration. This is consistent with the experimental result that the reaction has a first-order dependence on styrene concentration. The N–C bond formation occurs through a four-center planar structure TS'_1 involving a metal-mediated migratory insertion of the styrene C=C linkage into the Ln–N pyrroline σ bond. Following the reaction, TS'_1 decays to a metal alkyl intermediate III' . The olefin insertion step is endothermic, suggesting that the migratory olefin insertion is reversible. The additional coordination of pyrrolidine to III' , generating $\text{III}'\cdot\text{A}'$, drives the thermodynamics of the reaction (exothermic step) and is hardly affected by the pyrrolidine concentration (Table 4). Protonolytic cleavage of the metal carbon bond occurs through a metathesis-type transition state TS'_2 . The associated activation barriers (Sc: 16.4 kcal/mol, Y: 16.3 kcal/mol, and Pr: 16.2 kcal/mol) are almost the same and higher than those of their corresponding olefin insertion steps (Sc: 12.1 kcal/mol, Y: 15.6 kcal/mol, and Pr: 9.1 kcal/mol), suggesting that protonolysis should be the turnover-limiting step. This result is consistent with that observed in IEHA catalyzed by an alkaline-earth metal complex.⁷² It is worth noting that the equilibrium constant K_{298} for this protonolysis step is only 1.965 for the Pr-based catalyst calculated using the following equation

$$K = \exp\left(-\frac{\Delta G^\ddagger}{RT}\right)$$

suggesting that it is difficult to generate the product. With the decrease of the metal radius, the equilibrium constant becomes larger (Y: 311.61 and Sc: 4.17×10^4), indicating that the reaction degree was dramatically improved. Thus, the IEHA is under thermodynamic control.

CONCLUSIONS

The entire range of rare-earth metal bisalkyl complexes stabilized by the pyridine methylene fluorenyl ligand was, respectively, used to catalyze the IAHA of 1-amino-2,2-diphenyl-4-pentene and IEHA of styrene and pyrrolidine. As observed for all the reported rare-earth metal-based catalytic systems, the rate of the IAHA reaction increased almost linearly with the metal ion radius. The reactivity pattern in the IEHA reaction with respect to the ionic radius size followed the opposite trend to that of the IAHA reaction. DFT calculations suggest the prevailing mechanism to be a stepwise σ -insertive pathway that involves the insertion of C=C into the Ln–N bond and protonolysis of the Ln–C bond, regardless of intramolecular or intermolecular hydroamination. The activation barrier of protonolysis is higher than that of the insertion step, suggesting that the former reaction should be the turnover-limiting step. The protonolysis step was facilitated by an additional molecule of amine. Thus, the coordination of the amine to the insertion product is one of the key factors that control the hydroamination reaction. Two key aspects can be derived: (1) either the formation of the amine adduct is endothermic due to the crowded coordination sphere around the metal center, increasing the transition-state energy of the protonolysis step and a first-order dependence on the concentration of amine, such as the catalytic system reported by Sadow;³⁰ (2) or the amine coordination is thermodynamically preferred, resulting in lowering the transition-state energy of the protonolysis step. In the latter, a zero-order dependence on the amine is observed, such as IAHA catalyzed by yttrium and praseodymium base complexes. Since the coordination of aminoalkene to the scandium insertion product is nearly thermoneutral, the population of the aminoalkene adduct is rather low to limit the protonolysis reaction, resulting in the lowest activity of scandium species toward IAHA. Moreover, the enthalpy of protonolysis is another key factor that controls the hydroamination reaction. For the IEHA, with the increase of the metal radius, the aminolysis tends to be thermoneutral, leading to the left shift of the equilibrium and therefore a decrease of the catalytic activity following a trend of Sc > Y > Pr. The above systematic investigation fundamentally resolved the controversial issues toward hydroamination mediated by rare-earth metal catalysts and will be helpful to rationally design catalysts.

The authors declare no competing financial interest.

ASSOCIATED CONTENT

Supporting Information

The Supporting Information is available free of charge at <https://pubs.acs.org/doi/10.1021/acscatal.1c00566>.

Experimental section, ¹H NMR spectra of intramolecular and intermolecular hydroamination reaction, and the details of DFT calculation (PDF)

AUTHOR INFORMATION

Corresponding Authors

Laurent Maron – LPCNO, University of Toulouse, Toulouse 31077, France; orcid.org/0000-0003-2653-8557;

Email: laurent.maron@irsamc.ups-tlse.fr

Bo Liu – State Key Laboratory of Polymer Physics and Chemistry, Changchun Institute of Applied Chemistry, Chinese Academy of Sciences, Changchun 130022, China; University of Science and Technology of China, Hefei

230026, Anhui, China; orcid.org/0000-0002-8676-4794; Phone: +8643185262774; Email: liubo@ciac.ac.cn; Fax: (+86) 43185262774

Authors

Shuqi Dong – State Key Laboratory of Polymer Physics and Chemistry, Changchun Institute of Applied Chemistry, Chinese Academy of Sciences, Changchun 130022, China; University of Science and Technology of China, Hefei 230026, Anhui, China

Jinjin Chen – Key Laboratory for Green Organic Synthesis and Application of Hunan Province, Key Laboratory of Environmentally Friendly Chemistry and Application of Ministry of Education, College of Chemistry, Xiangtan University, Xiangtan 411105, China

Kening Qiao – Key Laboratory of Nonferrous Metal Chemistry and Resources Utilization of Gansu Province School of Chemistry and Chemical Engineering, Lanzhou University, Lanzhou 730000, P. R. China

Jian Fang – Key Laboratory of Nonferrous Metal Chemistry and Resources Utilization of Gansu Province School of Chemistry and Chemical Engineering, Lanzhou University, Lanzhou 730000, P. R. China

Yan Yang – LPCNO, University of Toulouse, Toulouse 31077, France

Complete contact information is available at: <https://pubs.acs.org/10.1021/acscatal.1c00566>

Author Contributions

#S.D. and J.C. contributed equally to this work.

Notes

The authors declare no competing financial interest.

ACKNOWLEDGMENTS

This work was supported by the NSF China with Projects No. 51673184. L.M. is a senior member of the Institut Universitaire de France. CalMip is acknowledged for a generous grant of computing time.

REFERENCES

- (1) Reznichenko, A. L.; Nawara-Hultzs, A. J.; Hultzs, K. C., Asymmetric Hydroamination. *Stereoselective Formation of Amines*; Springer: Berlin, 2014; 191–260.
- (2) Trowbridge, A.; Walton, S. M.; Gaunt, M. J. New Strategies for the Transition-Metal Catalyzed Synthesis of Aliphatic Amines. *Chem. Rev.* **2020**, *120*, 2613–2692 and reference therein.
- (3) Huang, L.; Arndt, M.; Gooßen, K.; Heydt, H.; Gooßen, L. J. Late Transition Metal-Catalyzed Hydroamination and Hydroamidation. *Chem. Rev.* **2015**, *115*, 2596–2697.
- (4) Li, Y.; Cheng, Y.; Shan, C.; Zhang, J.; Xu, D.; Bai, R.; Qu, L.; Lan, Y. Recent Advances in Alkaline-Earth-Metal-Catalyzed Hydrofunctionalization Reactions. *Chin. J. Org. Chem.* **2018**, *38*, 1885–1896.
- (5) Hill, M. S.; Liptrot, D. J.; Weetman, C. Alkaline Earths as Main Group Reagents in Molecular Catalysis. *Chem. Soc. Rev.* **2016**, *45*, 972–988.
- (6) Brinkmann, C.; Barrett, A. G. M.; Hill, M. S.; Procopiu, P. A. Heavier Alkaline Earth Catalysts for the Intermolecular Hydroamination of Vinylarenes, Dienes, and Alkynes. *J. Am. Chem. Soc.* **2012**, *134*, 2193–2207.
- (7) Arrowsmith, M.; Hill, M. S.; Kociok-Köhn, G. Bis(imidazolin-2-ylidene-1-yl)borate Complexes of the Heavier Alkaline Earths: Synthesis and Studies of Catalytic Hydroamination. *Organometallics* **2009**, *28*, 1730–1738.
- (8) Li, Z.; Zhang, J.; Brouwer, C.; Yang, C.-G.; Reich, N. W.; He, C. Brønsted Acid Catalyzed Addition of Phenols, Carboxylic Acids, and Tosylamides to Simple Olefins. *Org. Lett.* **2006**, *8*, 4175–4178.
- (9) Shapiro, N. D.; Rauniyar, V.; Hamilton, G. L.; Wu, J.; Toste, F. D. Asymmetric Additions to Dienes Catalysed by a Dithiophosphoric Acid. *Nature* **2011**, *470*, 245–249.
- (10) Li, Y.; Marks, T. J. Diverse Mechanistic Pathways and Selectivities in Organo-f-Element-Catalyzed Hydroamination. Intermolecular Organolanthanide-Catalyzed Alkyne and Alkene Hydroamination. *Organometallics* **1996**, *15*, 3770–3772.
- (11) Gagné, M. R.; Marks, T. J. Organolanthanide-Catalyzed Hydroamination. Facile, Regiospecific Cyclization of Unprotected Amino Olefins. *J. Am. Chem. Soc.* **1989**, *111*, 4108–4109.
- (12) Kim, Y. K.; Livinghouse, T.; Bercaw, J. E. Intramolecular Alkene Hydroaminations Catalyzed by Simple Amido Derivatives of the Group 3 Metals. *Tetrahedron Lett.* **2001**, *42*, 2933–2935.
- (13) Gagné, M. R.; Stern, C. L.; Marks, T. J. Organolanthanide-Catalyzed Hydroamination. A Kinetic, Mechanistic, and Diastereoselectivity Study of the Cyclization of N-Unprotected Amino Olefins. *J. Am. Chem. Soc.* **1992**, *114*, 275–294.
- (14) Ryu, J.-S.; Marks, T. J.; McDonald, F. E. Organolanthanide-Catalyzed Intramolecular Hydroamination/Cyclization of Amines Tethered to 1,2-Disubstituted Alkenes. *Org. Lett.* **2001**, *3*, 3091–3094.
- (15) Kim, Y. K.; Livinghouse, T. Exceptional Rate Enhancements and Improved Diastereoselectivities through Chelating Diamide Coordination in Intramolecular Alkene Hydroaminations Catalyzed by Yttrium and Neodymium Amido Complexes. *Angew. Chem., Int. Ed.* **2002**, *41*, 3645–3647.
- (16) Kim, Y. K.; Livinghouse, T.; Horino, Y. Chelating Bis-(thiophosphinic amidate)s as Versatile Supporting Ligands for the Group 3 Metals. An Application to the Synthesis of Highly Active Catalysts for Intramolecular Alkene Hydroamination. *J. Am. Chem. Soc.* **2003**, *125*, 9560–9561.
- (17) Hong, S.; Tian, S.; Metz, M. V.; Marks, T. J. C₂-Symmetric Bis(oxazolinato)lanthanide Catalysts for Enantioselective Intramolecular Hydroamination/Cyclization. *J. Am. Chem. Soc.* **2003**, *125*, 14768–14783.
- (18) O'Shaughnessy, P. N.; Knight, P. D.; Morton, C.; Gillespie, K. M.; Scott, P. Chiral-at-Metal Organolanthanides: Enantioselective Aminoalkene Hydroamination/Cyclisation with Non-Cyclopentadienyls. *Chem. Commun.* **2003**, 1770–1771.
- (19) Gribkov, D. V.; Hultzs, K. C. Kinetic Resolution of Chiral Aminoalkenes via Asymmetric Hydroamination/Cyclisation Using Binaphtholate Yttrium Complexes. *Chem. Commun.* **2004**, 730–731.
- (20) Kim, J. Y.; Livinghouse, T. Chelating Diamide Based Rate Enhancement of Intramolecular Alkene Hydroaminations Catalyzed by a Neutral Sc(III) Complex. *Org. Lett.* **2005**, *7*, 4391–4393.
- (21) Hultzs, K. C.; Gribkov, D. V.; Hampel, F. Non-Metallocene Rare Earth Metal Catalysts for the Diastereoselective and Enantioselective Hydroamination of aminoalkenes. *J. Organomet. Chem.* **2005**, *690*, 4441–4452.
- (22) Meyer, N.; Zulus, A.; Roesky, P. W. A Chiral-Bridged Aminotroponimate Complex of Lutetium as Catalyst for the Asymmetric Hydroamination. *Organometallics* **2006**, *25*, 4179–4182.
- (23) Bambirra, S.; Tsurugi, H.; Leusen, D.; Hessen, B. Neutral Versus Cationic Group 3 Metal Alkyl Catalysts: Performance in Intramolecular Hydroamination/Cyclisation. *Dalton Trans.* **2006**, 1157–1161.
- (24) Aillaud, I.; Collin, J.; Duhayon, C.; Guillot, R.; Lyubov, D.; Schulz, E.; Trifonov, A. New Chiral Lanthanide Amide Ate Complexes for the Catalysed Synthesis of Scalemic Nitrogen-Containing Heterocycles. *Chem. – Eur. J.* **2008**, *14*, 2189–2200.
- (25) Reznichenko, A. L.; Hampel, F.; Hultzs, K. C. Kinetic Resolution of Aminoalkenes by Asymmetric Hydroamination: A Mechanistic Study. *Chem. – Eur. J.* **2009**, *15*, 12819–12827.
- (26) Pawlikowski, A. V.; Ellern, A.; Sadow, A. D. Ligand Exchange Reactions and Hydroamination with Tris(oxazolinyl)borato Yttrium Compounds. *Inorg. Chem.* **2009**, *48*, 8020–8029.

- (27) Xu, X.; Chen, Y.; Feng, J.; Zou, G.; Sun, J. Half-Sandwich Indenyl Rare Earth Metal Dialkyl Complexes: Syntheses, Structures, and Catalytic Activities of $(1,3-(\text{SiMe}_3)_2\text{C}_9\text{H}_5)_\text{Ln}(\text{CH}_2\text{SiMe}_2)_2(\text{THF})$. *Organometallics* **2010**, *29*, 549–553.
- (28) Roux, E. L.; Liang, Y.; Storz, M. P.; Anwender, R. Intramolecular Hydroamination/Cyclization of Aminoalkenes Catalyzed by $\text{Ln}[\text{N}(\text{SiMe}_3)_2]_3$ Grafted onto Periodic Mesoporous Silicas. *J. Am. Chem. Soc.* **2010**, *132*, 16368–16371.
- (29) Lovick, H. M.; An, D. K.; Livinghouse, T. S. Structure–Activity Relationships in Group 3 Metal Catalysts for Asymmetric Intramolecular Alkene Hydroamination. An Investigation of Ligands Based on the Axially Chiral 1,1'-binaphthyl-2,2'-diamine motif. *Dalton Trans.* **2011**, *40*, 7697–7700.
- (30) Manna, K.; Kruse, M. L.; Sadow, A. D. Concerted C–N/C–H Bond Formation in Highly Enantioselective Yttrium(III)-Catalyzed Hydroamination. *ACS Catal.* **2011**, *1*, 1637–1642.
- (31) Lauterwasser, F.; Hayes, P. G.; Piers, W. E.; Schafer, L. L.; Brsea, S. Highly Active and Diastereoselective N,O- and N,N-Yttrium Complexes for Intramolecular Hydroamination. *Adv. Synth. Catal.* **2011**, *353*, 1384–1390.
- (32) Reznichenko, A. L.; Hultzsich, K. C. C_1 -Symmetric Rare-Earth Metal Aminodiolate Complexes for Intra and Intermolecular Asymmetric Hydroamination of Alkenes. *Organometallics* **2013**, *32*, 1394–1408.
- (33) Lyubov, D. M.; Luconi, L.; Rossin, A.; Tuci, G.; Cherkasov, A. V.; Fukin, G. K.; Giambastiani, G.; Trifonov, A. A. Metal-to-Ligand Alkyl Migration Inducing Carbon–Sulfur Bond Cleavage in Dialkyl Yttrium Complexes Supported by Thiazole-Containing Amidopyridinate Ligands: Synthesis, Characterization, and Catalytic Activity in the Intramolecular Hydroamination Reaction. *Chem. – Eur. J.* **2014**, *20*, 3487–3499.
- (34) Eedugurala, N.; Wang, Z.; Yan, K.; Boteju, K. C.; Chaudhary, U.; Kobayashi, T.; Ellern, A.; Slowing, I. L.; Pruski, M.; Sadow, A. D. β -SiH-Containing Tris(silazido) Rare-Earth Complexes as Homogeneous and Grafted Single-Site Catalyst Precursors for Hydroamination. *Organometallics* **2017**, *36*, 1142–1153.
- (35) Motolko, K. S. A.; Emslie, D. J. H.; Jenkins, H. A. Yttrium and Aluminum Alkyl Complexes of a Rigid Bis-Anilido NON-Donor Ligand: Synthesis and Hydroamination Catalysis. *Organometallics* **2017**, *36*, 1601–1608.
- (36) Kazeminejad, N.; Munzel, D.; Gamer, M. T.; Roesky, P. W. Bis(amidinate) Ligands in Early Lanthanide Chemistry–Synthesis, Structures, and Hydroamination Catalysis. *Chem. Commun.* **2017**, *53*, 1060–1063.
- (37) Nguyen, H. N.; Lee, H.; Audörsch, S.; Reznichenko, A. L.; Nawara-Hultzsich, A. J.; Schmidt, B.; Hultzsich, K. C. Asymmetric Intra- and Intermolecular Hydroamination Catalyzed by 3,3'-Bis(trisarylsilyl)- and 3,3'-Bis(arylalkylsilyl)-Substituted Binaphtholate Rare-Earth-Metal Complexes. *Organometallics* **2018**, *37*, 4358–4379.
- (38) Li, Y.; Marks, T. J. Organolanthanide-Catalyzed Intramolecular Hydroamination/Cyclization of Aminoalkynes. *J. Am. Chem. Soc.* **1996**, *118*, 9295–9306.
- (39) Li, Y.; Marks, T. J. Organolanthanide-Catalyzed Intra- and Intermolecular Tandem C–N and C–C Bond-Forming Processes of Aminodialkenes, Aminodialkynes, Aminoalkenynes, and Aminoalkynes. New Regiospecific Approaches to Pyrrolizidine, Indolizidine, Pyrrole, and Pyrazine Skeletons. *J. Am. Chem. Soc.* **1998**, *120*, 1757–1771.
- (40) Burgstein, M. R.; Berberich, H.; Roesky, P. W. (Aminotroponiminato)yttrium Amides as Catalysts in Alkyne Hydroamination. *Organometallics* **1998**, *17*, 1452–1454.
- (41) Hultzsich, K. C.; Hampel, F.; Wagner, T. New Yttrium Complexes Bearing Diamidoamine Ligands as Efficient and Diastereoselective Catalysts for the Intramolecular Hydroamination of Alkenes and Alkynes. *Organometallics* **2004**, *23*, 2601–2612.
- (42) Kim, H.; Livinghouse, T.; Shim, J. H.; Lee, S. G.; Lee, P. H. Yttrium(III)-Catalyzed Intramolecular Alkyne Hydroaminations. *Adv. Synth. Catal.* **2006**, *348*, 701–704.
- (43) Motolko, K. S. A.; Emslie, D. J. H.; Britten, J. F. Rigid NON-Donor Pincer Ligand Complexes of Lutetium and Lanthanum: Synthesis and Hydroamination Catalysis. *RSC Adv.* **2017**, *7*, 27938–27945.
- (44) Arredondo, V. M.; McDonald, F. E.; Marks, T. J. Organolanthanide-Catalyzed Intramolecular Hydroamination/Cyclization of Aminoallenes. *J. Am. Chem. Soc.* **1998**, *120*, 4871–4872.
- (45) Arredondo, V. M.; Tian, S.; McDonald, F. E.; Marks, T. J. Organolanthanide-Catalyzed Hydroamination/Cyclization. Efficient Allene-Based Transformations for the Syntheses of Naturally Occurring Alkaloids. *J. Am. Chem. Soc.* **1999**, *121*, 3633–3639.
- (46) Arredondo, V. M.; McDonald, F. E.; Marks, T. J. Intramolecular Hydroamination/Cyclization of Aminoallenes Catalyzed by Organolanthanide Complexes. Scope and Mechanistic Aspects. *Organometallics* **1999**, *18*, 1949–1960.
- (47) Hong, S.; Marks, T. J. Highly Stereoselective Intramolecular Hydroamination/Cyclization of Conjugated Aminodienes Catalyzed by Organolanthanides. *J. Am. Chem. Soc.* **2002**, *124*, 7886–7887.
- (48) Hong, S.; Kawaoka, A. M.; Marks, T. J. Intramolecular Hydroamination/Cyclization of Conjugated Aminodienes Catalyzed by Organolanthanide Complexes. Scope, Diastereo- and Enantioselectivity, and Reaction Mechanism. *J. Am. Chem. Soc.* **2003**, *125*, 15878–15892.
- (49) Aillaud, I.; Olier, C.; Chapurina, Y.; Collin, J.; Schulz, E.; Guillot, R.; Hannedouche, J.; Trifonov, A. Alkyl Complexes of Lanthanum and Samarium Supported by a Chiral Binaphthylamido Ligand. Syntheses, Structures, and Catalytic Activity in Hydroamination of Amino-1,3-dienes. *Organometallics* **2011**, *30*, 3378–3385.
- (50) Hangaly, N. K.; Petrov, A. R.; Rufanov, K. A.; Harms, K.; Elfferding, M.; Sundermeyer, J. Cyclopentadienylphosphazene (CpPN) Complexes of Rare-Earth Metals: Synthesis, Structural Characterization, and Hydroamination Catalysis. *Organometallics* **2011**, *30*, 4544–4554.
- (51) Stubbert, B. D.; Marks, T. J. Organolanthanide-Catalyzed Regioselective Intermolecular Hydroamination of Alkenes, Alkynes, Vinylarenes, Di- and Trivinylarenes, and Methylene-cyclopropanes. Scope and Mechanistic Comparison to Intramolecular Cyclohydroaminations. *J. Am. Chem. Soc.* **2003**, *125*, 12584–12605.
- (52) Gribkov, D. V.; Hultzsich, K. C.; Hampel, F. 3,3'-Bis(trisarylsilyl)-Substituted Binaphtholate Rare Earth Metal Catalysts for Asymmetric Hydroamination. *J. Am. Chem. Soc.* **2006**, *128*, 3748–3759.
- (53) Reznichenko, A. L.; Nguyen, H. N.; Hultzsich, K. C. Asymmetric Intermolecular Hydroamination of Unactivated Alkenes with Simple Amines. *Angew. Chem., Int. Ed.* **2010**, *49*, 8984–8987.
- (54) Germain, S.; Schulz, E.; Hannedouche, J. Anti-Markovnikov Hydroamination of Aromatic Alkenes with Secondary Amines Catalyzed by Easily Accessible Yttrium Complexes. *ChemCatChem* **2014**, *6*, 2065–2073.
- (55) Motta, A.; Lanza, G.; Fragala, I. L. Energetics and Mechanism of Organolanthanide-Mediated Aminoalkene Hydroamination/Cyclization. A Density Functional Theory Analysis. *Organometallics* **2004**, *23*, 4097–4104.
- (56) Tobisch, S. Organolanthanide-Mediated Intramolecular Hydroamination/Cyclization of Conjugated Aminodienes: A Computational Exploration of Diverse Mechanistic Pathways for the Regioselective Generation of Functionalized Azacycles Supported by a Lanthanocene-Based Catalyst Complex. *J. Am. Chem. Soc.* **2005**, *127*, 11979–11988.
- (57) Lin, F.; Wang, X.; Pan, Y.; Wang, M.; Liu, B.; Luo, Y.; Cui, D. Nature of the Entire Range of Rare Earth Metal-Based Cationic Catalysts for Highly Active and Syndioselective Styrene Polymerization. *ACS Catal.* **2015**, *6*, 176–185.
- (58) Otero, A.; Lara-Sanchez, A.; Castro-Osma, J.; Marquez-Segovia, I.; Alonso-Moreno, C.; Fernandez-Baeza, J.; Sanchez-Barba, L. F.; Rodriguez, A. M. Synthesis and structural characterization of amido heteroscorpionate rare-earth metal complexes and hydroamination of aminoalkenes. *New J. Chem.* **2015**, *39*, 7672–7681.

(59) Trambitas, A. G.; Panda, T. K.; Jenter, J.; Roesky, P. W.; Daniliuc, C.; Hrib, C. G.; Jones, P. G.; Tamm, M. Rare-Earth Metal Alkyl, Amido, and Cyclopentadienyl Complexes Supported by Imidazolin-2-iminato Ligands: Synthesis, Structural Characterization, and Catalytic Application. *Inorg. Chem.* **2010**, *49*, 2435–2446.

(60) Yu, X.; Marks, T. J. Organophosphine Oxide/Sulfide-Substituted Lanthanide Binaphtholate Catalysts for Enantioselective Hydroamination/Cyclization. *Organometallics* **2007**, *26*, 365–376.

(61) Trambitas, A. G.; Melcher, D.; Hartenstein, L.; Roesky, P. W.; Daniliuc, C.; Jones, P. G.; Tamm, M. Bis(imidazolin-2-iminato) Rare Earth Metal Complexes: Synthesis, Structural Characterization, and Catalytic Application. *Inorg. Chem.* **2012**, *51*, 6753–6761.

(62) Chai, Z.; Hua, D.; Li, K.; Zhou, S.; Chu, J.; Yang, G. Rare-earth metal complexes with tridentate linked amido-indenyl ligand: Synthesis, characterization, and catalytic properties for intramolecular hydroamination. *J. Organomet. Chem.* **2014**, *768*, 136–139.

(63) Rasttter, M.; Zulus, A.; Roesky, P. W. Bis(phosphinimino)-methanide Rare Earth Amides: Synthesis, Structure, and Catalysis of Hydroamination/Cyclization, Hydrosilylation, and Sequential Hydroamination/Hydrosilylation. *Chem. – Eur. J.* **2007**, *13*, 3606–3616.

(64) Hannedouche, J.; Collin, J.; Trifonov, A.; Schulz, E. Intramolecular Enantioselective Hydroamination Catalyzed by Rare Earth Binaphthylamides. *J. Organomet. Chem.* **2011**, *696*, 255–262.

(65) Hultzsck, K. C. Catalytic Asymmetric Hydroamination of Non-Activated Olefins. *Org. Biomol. Chem.* **2005**, *3*, 1819–1824.

(66) Stubbert, B. D.; Marks, T. J. Constrained Geometry Organoactinides as Versatile Catalysts for the Intramolecular Hydroamination/Cyclization of Primary and Secondary Amines Having Diverse Tethered C-C Unsaturation. *J. Am. Chem. Soc.* **2007**, *129*, 4253–4271.

(67) Liu, B.; Roisnel, T.; Carpentier, J.-F.; Sarazin, Y. Cyclohydroamination of Aminoalkenes Catalyzed by Disilazide Alkaline-Earth Metal Complexes: Reactivity Patterns and Deactivation Pathways. *Chem. – Eur. J.* **2013**, *19*, 2784–2802.

(68) Liu, B.; Roisnel, T.; Carpentier, J.-F.; Sarazin, Y. Heteroleptic Alkyl and Amide Iminoanilide Alkaline Earth and Divalent Rare Earth Complexes for the Catalysis of Hydrophosphination and (Cyclo)-Hydroamination Reactions. *Chem. – Eur. J.* **2013**, *19*, 13445–13462.

(69) Liu, B.; Roisnel, T.; Carpentier, J.-F.; Sarazin, Y. When Bigger Is Better: Intermolecular Hydrofunctionalizations of Activated Alkenes Catalyzed by Heteroleptic Alkaline Earth Complexes. *Angew. Chem., Int. Ed.* **2012**, *51*, 4943–4946.

(70) Tobisch, S. Organolanthanide-Mediated Intermolecular Hydroamination of 1,3-Dienes: Mechanistic Insights from a Computational Exploration of Diverse Mechanistic Pathways for the Stereoselective Hydroamination of 1,3-Butadiene with a Primary Amine Supported by an ansa-Neodymocene-Based Catalyst. *Chem. – Eur. J.* **2005**, *11*, 6372–6385.

(71) Tobisch, S. Mechanistic elucidation of the yttrium(III)-catalysed intramolecular aminoalkene hydroamination: DFT favours a stepwise σ -insertive mechanism. *Dalton Trans.* **2012**, *41*, 9182–9191.

(72) Tobisch, S. Intermolecular Hydroamination of Vinylarenes by Iminoanilide Alkaline-Earth Catalysts: A Computational Scrutiny of Mechanistic Pathways. *Chem. – Eur. J.* **2014**, *20*, 8988–9001.